Proceedings of MNHT2008
Micro/Nanoscale Heat Transfer International Conference
January 6-9, 2008, Tainan, Taiwan

MNHT 2008-52096

SESSILE DROP EVAPORATION ON SURFACES OF VARIOUS WETTABILITY

Hyunsoo Song
School of Mechanical and Aerospace Engineering
Seoul National University
Seoul
Korea

Yongku Lee
Faculty of Kinesiology
University of Calgary
Calgary, Alberta
Canada

Songwan Jin
Departments of Medicine and Physiology
University of California, San Francisco
California
USA

Ho-Young Kim
School of Mechanical and Aerospace Engineering
Seoul National University
Seoul
Korea

Jung Yul Yoo *
School of Mechanical and Aerospace Engineering
Seoul National University
Seoul
Korea

ABSTRACT

This work experimentally investigates the evaporation rates of water drops on surfaces of various wettability. By measuring the temporal evolutions of the drop radius and contact angle, we find the qualitative difference between the evaporation behavior on hydrophilic surfaces where the contact radius remains constant initially and that on the superhydrophobic surfaces where the contact angle remains constant. Also, the evaporation rate is observed to depend on the surface material although the currently available models assume that the rate is solely determined by the drop geometry. Although the theory to explain this dependence on the surface remains to be pursued by the future work, we give the empirical relations that can be used to predict the drop volume evolution for each surface.

Keywords: evaporation, contact angle, hydrophilic, superhydrophobic

NOMENCLATURE

A	area through which diffusion occurs (m^2)
c	vapor density (g/mm^3)
D	vapor diffusivity in still air (mm^2/s)
g	gravitational acceleration (m/s^2)
J	vapor flux per unit area ($g/s \cdot m^2$)
P	pressure (Pa)
q	evaporation rate (g/s)
Q	evaporation rate (g/s)
r	radial distance (m)
R	radius of drop curvature (m)
t	time (s)
V	drop volume (L)

Greek Symbols

α	distance from the contact line (m)
Λ	distance from the contact line (m)
ρ	liquid density (kg/m^3)
θ	contact angle (°)
σ	surface tension (N/m)
Bo	Bond number

Subscripts and superscripts

e	equilibrium
s	saturated

INTRODUCTION

A liquid drop sitting on a solid surface dries unless the entire surrounding is saturated with its vapor. The drop may decrease its volume by decreasing either its contact angle or contact area with the solid surface. When the solid wets the liquid, the contact line is pinned during evaporation in general

Table 1. Root mean square roughness and the equilibrium contact angle with water of the surfaces used in the experiments.

Surface	AKD	Glass	MEMS	OTS	Bare Si wafer	Sandblasted	Teflon	Thermal Si oxide	Platinum	Gold
Roughness (nm)	31.693	6.375	16.907	4.770	·	·	2.198	0.47	·	·
θ_e (°)	143.46	57.16	147.94	100.05	36.74	55.90	92.41	43.07	94.75	84.67

thus the contact angle alone decreases in the first stages [1,2]. In this case, a liquid flow is induced toward the drop edge to replenish the liquid evaporating there, which is known to cause ring stains left by dried drops that contain solid solutes like coffee [3]. In addition to this mundane example, drying drops play important roles in the lab-on-a-chip technology including DNA chips, where drops of DNA solutions are deposited on functionalized glass slides and left to react until they completely evaporate [4]. Moreover, it was found that DNA molecules could be highly stretched at the periphery of a drying drop of polymer solution placed on a glass cover-slip [5].

Major interests of studying the evaporation of a sessile drop lie in predicting the temporal evolutions of the drop shape and volume. They depend on the physical properties of the vapor, humidity of surrounding air and the physicochemical interaction of liquid with solid. The evaporation rate can bemathematically modeled assuming diffusive transport of vapor molecules into an infinite medium and the comparisons with experimental results were reported previously [1, 2]. We note here that most research efforts so far have been devoted to wetting surfaces on which the liquid drop has the contact angle less than 90°. However, increasingly many modern engineering surfaces interacting with liquid drops possess hydrophobicity. Many microfluidic devices are fabricated with low-surface-energy polymers by soft lithography [6]. In addition, solid surfaces with an extremely high water-repellency, i.e. superhydrophobic surfaces, are known to be highly effective in transporting liquid drops [7, 8].

Therefore, here we experimentally investigate the evaporation process of sessile water drops on surfaces not only hydrophilic but also hydrophobic. We compare our experimental results with the existing theories and discuss the validity of the models. Furthermore, we suggest empirical relations that can be used to predict the drop volume evolution with time for each surface material.

MATERIALS AND METHODS

We observed evaporation of deionized water drops on various materials of surfaces. As hydrophilic surfaces which have the equilibrium contact angle with water $\theta_e < 90°$, platinum, bare silicon, thermally grown silicon oxide, and sand-blasted glass were used. As hydrophobic surfaces having θ_e slightly greater than $90°$, a self-assembled monolayer of octadecyltrichlorosilane (OTS) and poly-tetrafluoroethylene

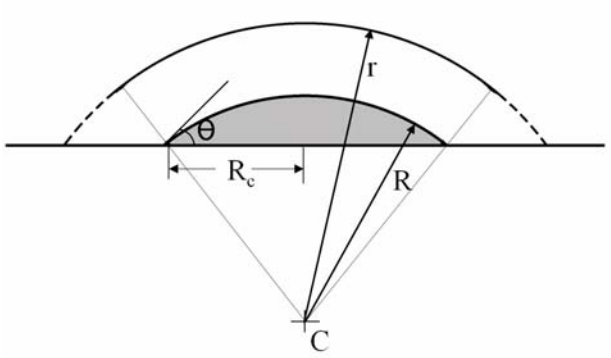

Fig. 1 Geometry of the sessile drop and diffusion area. The solid line at the distance *r* from the center of the curvature C represents the diffusion area modeled by [1]. The diffusion area modeled by [12] is represented by the dashed lines and the solid line at *r*.

(PTFE) were used. As superhydrophobic surfaces, AKD (alkyl dimer) and microfabricated structure were adopted. For the AKD surface, a chloroform-AKD mixture was sprayed onto a glass surface and left to dry for three hours. The values of θ_e and the roughness of the foregoing surfaces are listed in Table 1.

After placing a millimeter-sized water drop on the surface, images of an evaporating drop were taken every 20 seconds using a CCD camera periodically triggered by a computer. Temperature and relative humidity of the atmosphere were measured by ETL Digital Thermo-Hygrometer with the accuracy of 0.1°C and 1 % for temperature and relative humidity, respectively. During the experiments, temperature and relative humidity were maintained constant with variations less than 1°C and 1%, respectively. The vapor diffusivity and the saturated vapor density were calculated by the formulas given by Vargaftik [9] and Kimball et al. [10], respectively.

To measure the contact radius and the height of the drop from the images, we obtained five points on the drop/air interface and six points on the air/substrate interface using a simple threshold routine in image analysis software. Then the contact angle and the volume of the drop were deduced by assuming a spherical cap shape due to small Bond number, defined as $Bo = \rho g R^2 / \sigma$, where ρ being the liquid density, g the gravitational acceleration, R the radius of curvature, σ the surface tension. In our experiments, Bo was kept below 0.5. The evaporation rate was obtained by differentiating

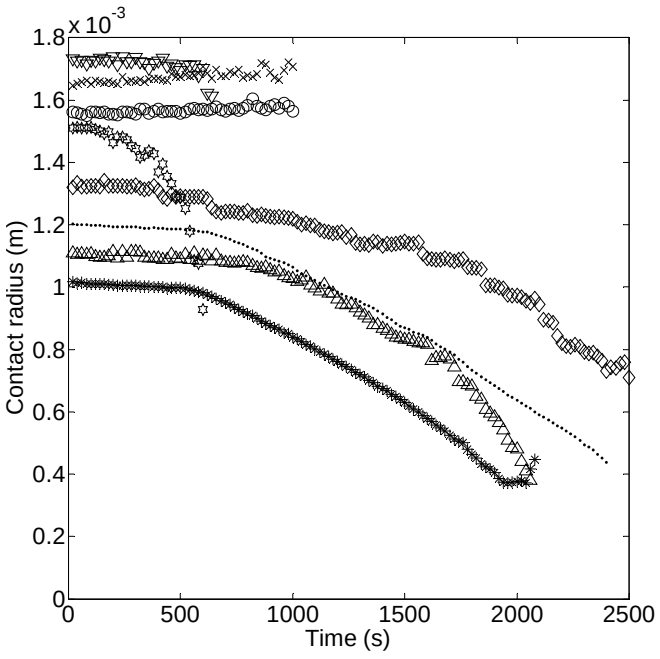

(a)

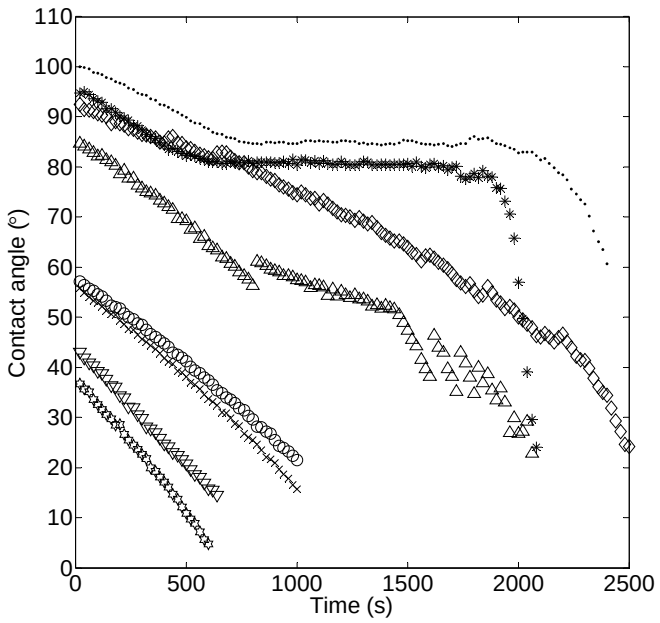

(b)

Fig. 2 The temporal evolutions of (a) the contact radius and (b) the contact angle on various surfaces. The dots correspond to the water drop on the OTS surface, stars Pt, diamonds PTFE, upright triangles gold, circles glass, crosses sandblasted glass, inverted triangles thermal oxide, and hexagrams bare Si wafer.

the drop volume with time after fitting the temporal evolution of the volume to the third-order polynomial in time with the least square method.

EVAPORATION ON HYDROPHILIC SURFACE

When a drop is situated on a solid surface, the adjacent air is saturated with vapor due to rapid interchange of liquid molecules [1]. The vapor in the thin saturated area diffuses outward into the surrounding unsaturated air. The evaporation rate of vapor, Q, is determined by Fick's law

$$Q = -DA\frac{dc}{dr} \tag{1}$$

where D is the vapor diffusivity in still air, A the area through which diffusion occurs, c the vapor density, and r the radial distance as illustrated in Fig. 1. Here we consider the vapor density gradient only in the radial direction. Assuming a quasi-equilibrium process for a slow evaporation in still air, we integrate Eq. 1 from the drop surface to infinity to give a drop volume change with time:

$$\frac{dV}{dt} = -\frac{4\pi DR}{\rho}\left(c_S - c_\infty\right) f(\theta) \tag{2}$$

where V is the drop volume, t the time, R the radius of the drop curvature, ρ the liquid density, c_s the saturated vapor density at drop surface, c_∞ the ambient vapor density determined by the relative humidity, and θ the contact angle assumed by a drop during evaporation. The function $f(\theta)$ is determined by the profile of area through which liquid molecules are assumed to diffuse. It is interesting to note that in this type of diffusion problem, the volume change is linearly proportional to the length scale (R) rather than the surface area.

To predict the temporal evolution of drop volume and shape, the value of $f(\theta)$ and how the contact radius R_c and contact angle θ behave with time should be known *a priori*. In figure 2, we show measured R_c and θ with time for different surfaces. In all the cases, R_c stays constant in the first stage while θ decreases with time. For some surfaces, R_c decreases later and this is interpreted as the receding of the contact line when θ reaches the critical receding angle θ_R. After R_c starts to decrease, θ remains the same on the platinum surface while it keeps decreasing on the PTFE surface. There seems to exist no theory to explain why the behavior of θ is different, while R_c decreases, depending on surface materials.

Since knowledge of $f(\theta)$ is one prerequisite for the accurate prediction of the drop volume change with time, various models were suggested thus far. Rowan et al. [1]

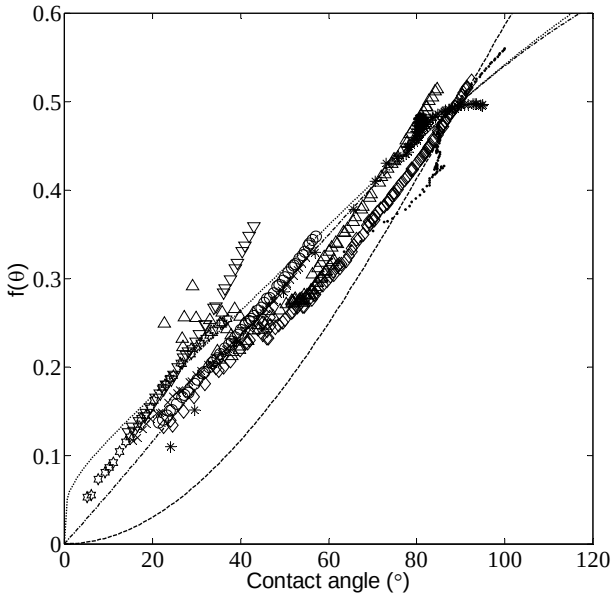

Fig. 3. $f(\theta)$ versus θ. The dashed line is from the model of [1], the dotted line from [12], and the dash-dotted line from [14]. The symbols correspond to the experimental results on the same surface as indicated in Fig. 2.

assumed that vapor molecules escape from a curved surface only at a radial direction thus the effective diffusion area A becomes as shown in Fig. 1. Then the area is written as $A = 2\pi r^2 (1-\cos\theta)$ and $\nabla^2 c = 0$. This model neglects the evaporation flux at the drop edge, which can be greater than that from the area far from the edge [11], thus needs a remedy. Bourges-Monnier and Shanahan [12] suggested a model in which the effective diffusion area entirely compasses the drop area as shown in Fig. 1. Then the effective diffusion area and $f(\theta)$ are respectively given by $A = 2\pi r^2 (1-R_s \cos\theta / r)$ and $f(\theta) = -\cos\theta / \left[2\ln(1-\cos\theta)\right]$. This model incorporates the diffusion area excluded by Ref. [1], thus the calculated evaporation rate is greater than that by the model of [1]. However, the increase of the radial distance leads to the increase of the central angle of the spherical cap in this model. This implies redistribution of vapor molecules in the azimuthal direction, contradictory to the assumption of pure radial density gradient. The evaporation rate modeled by [12] gives the maximum rate possible as long as the drop remains to be a part of a sphere.

The major difference of the models of Refs. [1] and [12] comes from how to treat evaporation around the drop edge where the liquid meets the solid. The steady-state diffusion equation, $\nabla^2 c = 0$, for the vapor concentration in the sharp wedge around the drop's contact line can be solved using the method of images [13]. Then the vapor flux per unit area, J, is given by

$$J \propto \alpha^{-\gamma} \tag{3}$$

where α is the distance from the contact line and $\gamma = (\pi - 2\theta)/(2\pi - 2\theta)$. Since γ is positive for hydrophilic surfaces ($\theta < \pi/2$), the vapor flux diverges as α approaches zero, i.e. near the contact line [3]. However, the evaporation rate, q, over a finite surface area extending a distance Λ from the contact line, which is obtained by integrating J, is bounded as shown in the following:

$$q \propto \int_0^{\Lambda} \alpha^{-\gamma} d\alpha \propto \Lambda^{1-\gamma} \tag{4}$$

where $\gamma < 1$ always. Although this edge effect may be small as compared with the bulk evaporation rate, ignoring (as in [1]) or overestimating (as in [12]) such an effect introduces an accumulation of errors that leads to a rather severe discrepancy between the theory and the experiment. As an alternative to the models of Refs. [1] and [12], the model of Picknett and Bexon [14] can be considered. They obtained $f(\theta)$ using the capacitance of the equiconvex lens formed by a sessile drop and its image. Thus obtained $f(\theta)$ lies between the results of Refs. [1] and [12] as shown in Fig. 3.

Therefore, it is naturally in order to investigate how $f(\theta)$ behaves on actual surfaces experimentally. The results are shown in Fig. 3 together with the foregoing theoretical models. It indicates that the dependence of f on θ strongly depends on the surface material thus the measurement data do not collapse to a single line. Furthermore, $f(\theta)$ on the thermally grown silicon oxide surface lies above the upper bound although the values of f on most surfaces remain between the upper bound suggested by [12] and the lower bound by [1]. Our experiments revealed that at the same contact angle rendering the same drop shape, the evaporation behavior is different depending on the surfaces. This indicates that the geometric consideration alone, as adopted in the foregoing models, cannot explain the differences of evaporation behavior on various surfaces. This leads us to consider the additional effects of solid surfaces on evaporation behavior besides the effect manifested by the contact angle. The effects may be caused by the existence of precursor films and adsorption of vapor molecules to the solid surface. Detailed studies on these aspects should follow in the future. Although none of the currently available theories accurately predict $f(\theta)$ on the various surfaces, our experiments indicate that all the surfaces exhibit approximately linear dependence of f on θ. Therefore, in Table 2, we give the best-fitting linear formulas of $f(\theta)$ for each surface. Using this formula can accurately predict the temporal drop volume evolution as shown in Fig. 4.

Table 2 Empirically determined linear relationship of $f(\theta)$ and θ as expressed by $f(\theta) = a \cdot \theta + b$. Here θ is in radian.

Surface	*a*	*b*
Glass	0.338	$6.4 \cdot 10^{-3}$
OTS	0.418	$-172.4 \cdot 10^{-3}$
Si wafer	0.372	$24.1 \cdot 10^{-3}$
Sandblasted	0.286	$38.2 \cdot 10^{-3}$
Teflon	0.327	$-21.3 \cdot 10^{-3}$
Thermal	0.464	$-5.3 \cdot 10^{-3}$
Platinum	0.315	$21.3 \cdot 10^{-3}$
Gold	0.286	$38.8 \cdot 10^{-3}$

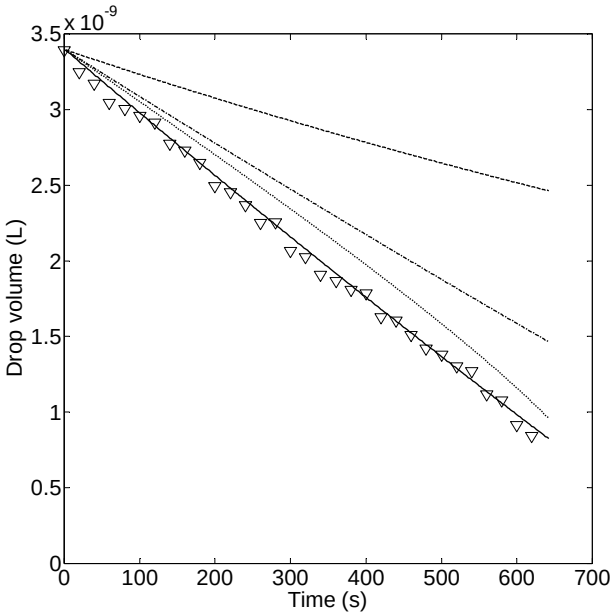

Fig. 4 Comparison of the predictions of the drop volume change with time and the experimental results on the thermal silicon oxide. The dashed, dotted and dash-dotted lines were obtained by using $f(\theta)$ as modeled as [1], [12] and [14], respectively. The solid line is from the current linear relationship of $f(\theta)$ and θ.

EVAPORATION ON SUPERHYDROPHOBIC SURFACE

To investigate evaporation behavior of sessile drops on superhydrophobic surfaces, we used AKD and microfabricated surfaces, whose scanning electron microscopy (SEMS) images are shown in Fig. 5. The most sensible difference of the evaporation on the superhydrophobic surfaces from that on hydrophilic surfaces is that the path of the vapor diffusion is eventually blocked by a solid if starting from the surface area below the drop's equator, as illustrated in Fig. 6. Therefore, instead of a diverging vapor flux near the contact line, the drop

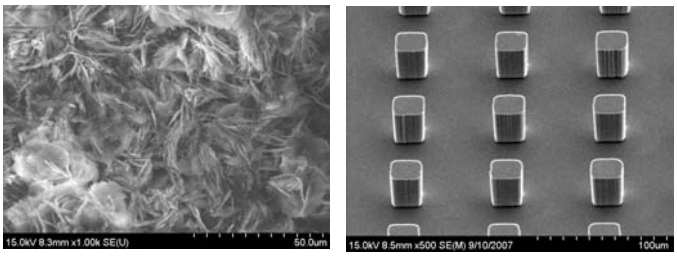

Fig. 5 SEM images of the superhydrophobic AKD (left) and microfabricated surface (right).

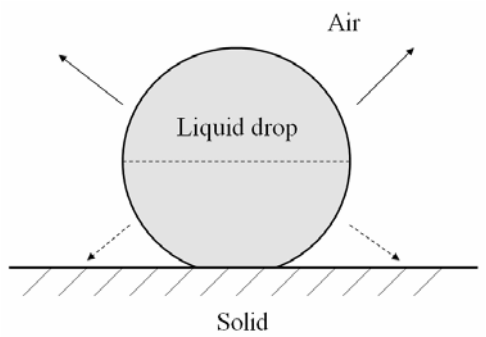

Fig. 6 Diffusion paths of water molecules on a superhydrophobic surface. The solid arrowed line extends to infinity, but the dotted arrowed line is blocked by the substrate.

on a superhydrophobic surface has a vanishing vapor flux in the edge. This can be mathematically explained by a relation (3),where $\gamma < 0$ for $\theta > \pi/2$.

Fig. 7 shows the temporal evolution of R_C and θ on the superhydrophobic surfaces, revealing that unlike the drops on hydrophilic surfaces, θ is maintained constant initially while R_c continuously decreases. In the superhydrophobic state, i.e. the Cassie state [15], the drop contacts only the top of asperities thus a very high contact angle over 150° is maintained. As the drop shrinks during evaporation, the Laplace pressure, inversely proportional to the drop radius, increases, thus the water begins to penetrate into interstices of the rough surface. This eventually causes the drop/solid contact behavior to enter the Wenzel state [16], where the rough surface is imbibed by the liquid. On both the hydrophobic surfaces, θ begins to drop when R_c reaches approximately $200\mu m$. The threshold Laplace pressure over which θ begins to drop is then given by $\Delta P = 2\sigma / R \approx 350$ Pa. This value is higher than the threshold pressure measured by Ref. [17] (~200 Pa) while separating the two plates between which the drop is squeezed. In addition, the receding contact angle dropped abruptly in the experiments of Ref. [17] while our evaporation experiments showed a gradual decrease of θ.

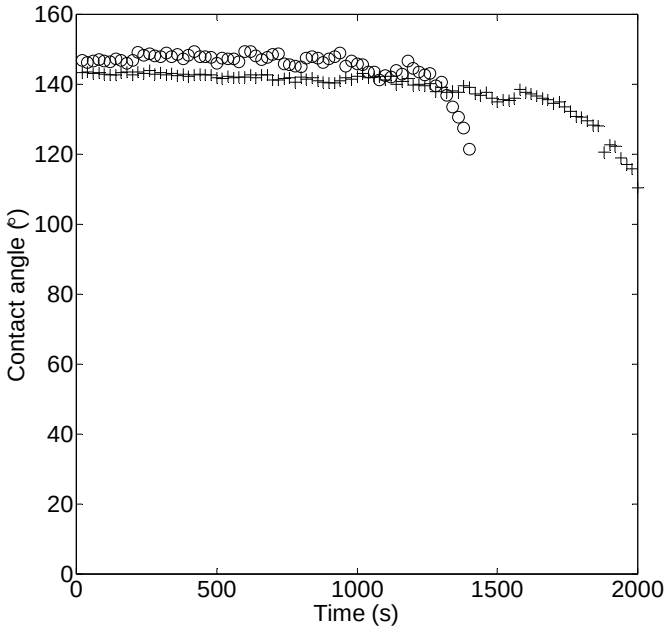

(a)

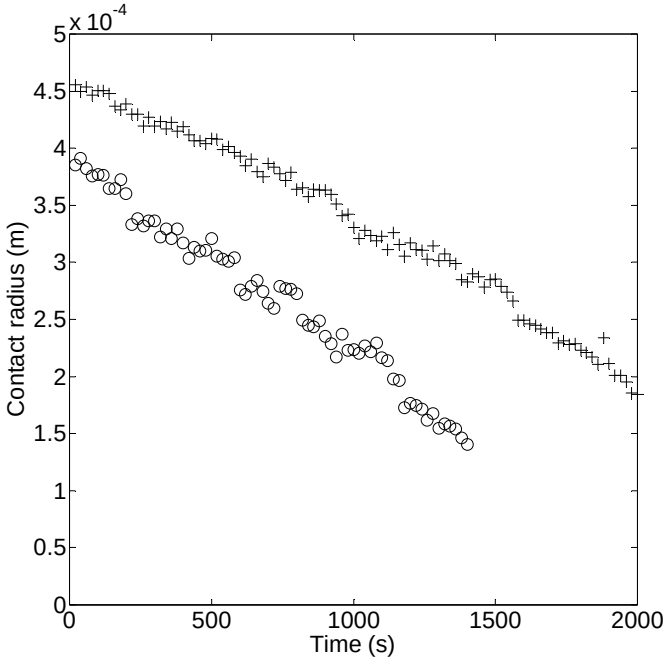

(b)

Fig. 7 The temporal evolutions of (a) the contact radius and (b) the contact angle on the hydrophobic surfaces. The circles correspond to the water drop on the microfabricated structure and crosses on the AKD surface.

We obtained $f(\theta)$ for the evaporation on the superhydrophobic surfaces in the same method as for the hydrophilic surfaces, and the results are shown in Fig. 8. The values lie below all the predictions by Refs. [1], [12] and [14].

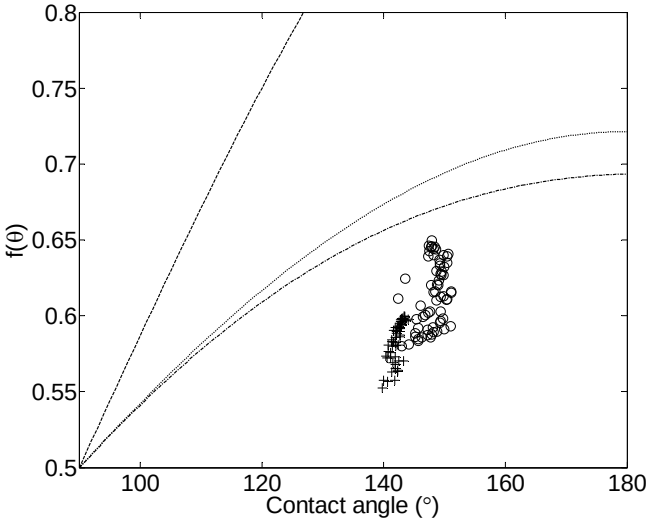

Fig. 8 $f(\theta)$ versus θ. The dashed line is from the model of [1], the dotted line from [12], and the dash-dotted line from [14]. The symbols correspond to the experimental results on the same surface as indicated in Fig. 7.

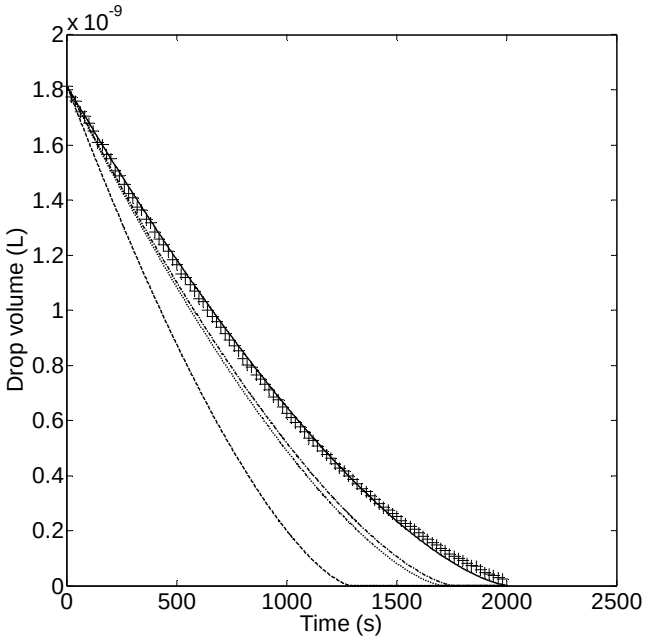

Fig. 9 Comparison of the predictions of the drop volume change with time and the experimental results on the AKD surface. The dashed, dotted and dash-dotted lines were obtained by using $f(\theta)$ as modeled as [1], [12] and [14], respectively. The solid line is calculated using the constant value of $f(\theta)$ as obtained by this work.

It is a natural consequence because both the diffusion areas considered by Refs. [1] and [12] include the area below vary little during evaporation, it is unrealistic to find a linear

empirical relationship between f and θ as in hydrophilic experiments. Thus we obtained the average value of f for each surface as f = 0.58 for AKD and f = 0.61 for the microfabricated surface. Fig. 9 shows that using a single value of f in the calculation of the drop volume evolution with time gives fairly accurate predictions of the experiments.

CONCLUSIONS

We experimentally studied the evaporation behavior of water drops on various surfaces covering a wide range of wettability. Although all the existing models predicted that the geometry, i.e. the contact radius and contact angle, determine the evaporation rate, our experimental results show that the evaporation rate depends on the surface condition as well as the drop geometry. Thus we obtained the linear empirical relationships for the evaporation rate on each surface, which enables fairly accurate prediction of the drop volume change on each surface. On the superhydrophobic surfaces, the drop was found to decrease its contact radius while the high contact angle is maintained. Upon the Laplace pressure exceeding a certain value, the contact angle starts to decrease gradually. Our results can guide research efforts toward investigating the physicochemical mechanism of solid surfaces affecting the evaporation rate.

ACKNOWLEDGMENTS

This work was supported by grant No. R01-2005-000-10558-0 from the Basic Research Program of the Korea Science & Engineering Foundation (KOSEF), and also by the Micro Thermal System Research Center under the auspices of KOSEF.

REFERENCES

[1] Rowan, S. M., Newton, M. I., and McHale, G. J., 1995, "Evaporation of Microdroplets and the Wetting of Solid Surfaces," J. Phys. Chem., 99, pp. 13268-13271.
[2] Erbil, H. Y., McHale, G., and Newton, M. I., 2002, "Drop Evaporation on Soid Surface: Constant Contact Angle Mode," Langmuir, 18, pp. 2636-2641.
[3] Deegan, R. D., Bakjin, O., Dupont, T. F., Huber, G., Nagel, S. R., and Witten, T. A., 1997, "Capillary flow as the cause of ring stains form dried liquid drops," Nature, 389, pp. 827-829.
[4] Dugas, V., Broutin, J., and Souteyrand, E., 2005, "Droplet Evaporation Study Applied to DNA Chip Manufacturing," Langmuir, 21, pp. 9130-9136.
[5] Abramchuk, S. S., Khokhlov, A. R., Iwataki, T., Oana, H., and Yoshikawa, K., 2001, "Direct observation of DNA molecules in a convection flow of a drying droplet," Europhys. Lett., 55(2), pp. 294-300.
[6] Xia, Y., and Whitesides, G. M., 1998, "Soft Lithography," Angew. Chem. Int. Ed., 37, 550-575.
[7] Mahadevan, L., and Pomeau, Y., 1999, "Rolling droplets," Phys. Fluids, 11, pp. 2449-2453.
[8] Callies, M., and Quéré, D., 2005, "On water repellency," soft matter, 1, pp. 55-61.
[9] Vargaftik, N. B., 1975, Tables on Thermophysical Properties of Liquids and Gases, Hemisphere, Washington D.C.
[10] Kimball, B. A., Jackson, R. D., Reginato, R. J., Nakayama, F. S., and Idso, S. B., 1976, "Comparison of field-measured and calculated soil-heat fluxes," soil Sci. Soc. Am. Proc., 40, pp. 18-25.
[11] Hu, H., and Larson, R. G., 2002, "Evaporation of a Sessile Droplet on a Substrate," J. Phys. Chem. B, 106, pp. 1334-1344.
[12] Bourges-Monnier, C., and Shanahan, M. E. R., 1995, "Influence of Evaporation on Contact Angle," Langmuir, 11, pp. 2820-2829.
[13] Jackson, J. D., 1975, Classical Elctrodynamics 2nd edn, Wiley, New York, USA
[14] Picknett, R. G., and Bexon, R, J., 1977, "The Evaporation of Sessile or Pendant Drops in Still Air," J. Colloid Interface Sci, 61, pp. 336-350.
[15] Cassie, A. B. D., and Baxter, S., 1944, "Wettability of porous surfaces," Trans. Faraday Soc., 40, pp. 546-551.
[16] Wenzel, R. N., 1936, "Resistance of solid surfaces to wetting by water," Ind. Eng. Chem., 28, pp. 988-994.
[17] Lafuma, A., and Quéré, D., 2003, "Superhydrophobic states," Nature Materials, 2, pp. 457-460.